A Dual-Band Coupled Resonator Decoupling Network for Two Coupled Antennas

Luyu Zhao, *Member, IEEE*, and Ke-Li Wu, *Fellow, IEEE*

***Abstract*—A new decoupling scheme called dual-band coupled resonator decoupling network (CRDN) is presented. By properly designing the coupling coefficients between two pairs of coupled resonators, the network can effectively reduce the mutual couplings between two coupled dual-band antennas in two bands simultaneously. The new scheme is proved by a practical microstrip version of the device for two dual-band antennas working at 2.4 and 5.2 GHz frequency bands. A compact planar dual-band CRDN consisting of a pair of dual-band open-loop square ring resonators is proposed. The measured scattering parameters of two coupled antennas with and without the dual-band CRDN in free space (FS) and with hand phantom demonstrate that the isolation between the two antennas in both the low and high bands can be improved from 8 to 10 dB, respectively, to below 20 dB while maintaining a good matching performance. The total efficiency and envelop correlation coefficient for the decoupled antennas show a significant improvement as compared to the coupled antenna case. The proposed dual-band CRDN scheme is easy to be implemented in an integrated device, and is very attractive for practical multiple input and multiple output (MIMO) applications.**

***Index Terms*—Compact antenna array, coupled resonators, decoupling network, dual-band, multiple input and multiple output (MIMO), mutual coupling.**

I. Introduction

NOWADAYS, more and more multistandard, multiband, and multimode wireless terminals with multiple antennas have become popular on the market. Such devices include various wireless routers as well as multimode 2G/3G and LTE smart phones and tablets. An obvious trend of these wireless terminals is the use of multiple antennas for multiple input and multiple output (MIMO) data access in a compact volume. When multiple antennas are installed in a size-constraint terminal, the physical limitation in separations of the antennas cannot be easily transcended without sacrificing system performances. Furthermore, hostile interferences through mutual couplings in the operating frequency bands become a bottleneck for further improving the data rate of wireless systems.

Manuscript received July 24, 2014; revised January 19, 2015; accepted March 18, 2015. Date of publication April 10, 2015; date of current version July 02, 2015. This work was supported in part by the Postgraduate scholarship of The Chinese University of Hong Kong and in part by the Development and Reform Commission of Shenzhen Municipality under Grant Shen Fa Gai (2013) 1673. *(Corresponding author: K.-L. Wu.)*

The authors are with the Department of Electronic Engineering, The Chinese University of Hong Kong, Shatin, Hong Kong and also with the Shenzhen Engineering Laboratory of Wireless Locating Technology and System, Shenzhen Research Institute, The Chinese University of Hong Kong, Shatin, Hong Kong (e-mail: lyzhao@ee.cuhk.edu.hk; klwu@ee.cuhk.edu.hk).

Color versions of one or more of the figures in this paper are available online at http://ieeexplore.ieee.org.

Digital Object Identifier 10.1109/TAP.2015.2421973

Significant attentions have been paid to mitigate the above-mentioned interferences in a multiple antenna system, which is termed as the antenna decoupling problem [1]–[12]. But such endeavors have been mostly constrained to single-band applications, which cannot fulfill the requirement for the multiband systems. For example, emerging long-term evolution (LTE) systems may operate in 700-MHz, 2.3-GHz, and 2.6-GHz bands, and the WLAN standards IEEE 802.11 a/b/g/n and ac operate at 2.4- and 5-GHz bands with an advanced option of at least 2×2 MIMO.

Many of the existing methods for dual-band decoupling problems simply extend the single-band decoupling method to the context of a dual-band problem. For example, [13] and [14] intend to decouple a pair of dual-band antennas operating at two bands (803–820 and 2440–2900 MHz in [13], UMTS (1920–2170 MHz), and WLAN (2400–2484 MHz) in [14]) with a defected ground structure (DGS), respectively. As it is known, DGSs are antenna-dependent and are not convenient for dual-band applications. Not to mention that the footprint of a DGS is quite large. Besides, these structures can have noticeable influence on the radiation patterns and efficiencies of the two antennas. The work in [15] uses an *ad hoc* structure to alter the current distribution of coupled antennas for decoupling two dual-band antennas. The structure is antenna-dependent and must be designed by intuition. Additionally, it is obvious that currents induced on the line affect the radiation pattern. Another scheme using a lumped element decoupling network for coupled dual-band antennas is also proposed in [16] and [17]. A dual-band version of mode-decomposition technique [18], [19] and a combination of this technique with a passive decoupling network technique [20] are also proposed. There are three obvious issues in [18]–[20]: the network size is large; the modes' Q and efficiency are different for different modes; and the insertion loss of the decoupling network is not negligible.

Recently, a new concept named coupled resonator decoupling network (CRDN) is proposed for wide-band decoupling of two or three element antenna arrays [11] and [12]. Based on the concept of CRDN for single-band applications, a dual-band decoupling technique using a dual-band CRDN is proposed in this paper. Comparing to the existing dual-band decoupling solutions, the proposed scheme has the following unique features.

1) The dual-band CRDN can take various form factors in realization, such as low temperature cofired ceramics (LTCC) and integrated passive devices (IPD), and can be integrated in a very compact volume.
2) The CRDN can be synthesized and designed according to specifications for given antenna characteristics.

3) Since a dual-band CRDN is a filter-like structure in nature, many advanced filter design methods can be directly inherited.

This paper is organized as follows. The working principle and basic design theory of the proposed dual-band CRDN will be presented in Section II followed by one proof-of-concept design example in Section III, in which a thorough investigation on the radiation performance of the decoupled array is conducted. Finally, conclusion is given in Section IV.

II. Working Principle and Design Theory

A. Network Model

Two closely spaced dual-band antennas of any form factor can be described by a two-port lossy network whose admittance matrix is $[\mathbf{Y}^A]$ with complex entries. To decouple the antennas, a dual-band CRDN constructed by a plurality of coupled resonators is connected to the antennas in shunt as shown in Fig. 1(a). Assuming that the admittance matrix of the CRDN is denoted by $[\mathbf{Y}^D]$, the total admittance matrix of the antenna array with the CRDN is the sum of the two individual admittance matrices as

$$\mathbf{Y}=\begin{bmatrix} Y_{11}(\omega) & Y_{12}(\omega) \\ Y_{21}(\omega) & Y_{22}(\omega) \end{bmatrix}=\begin{bmatrix} Y_{11}^A(\omega)+Y_{11}^D(\omega) & Y_{12}^A(\omega)+Y_{12}^D(\omega) \\ Y_{21}^A(\omega)+Y_{21}^D(\omega) & Y_{22}^A(\omega)+Y_{22}^D(\omega) \end{bmatrix} \tag{1}$$

where ω is the bandpass angular frequency.

Note that since the CRDN is considered as a lossless passive network, the entries of $[\mathbf{Y}^D]$ must be purely imaginary. It can be easily found from the S-to-Y transformation that to decouple the two dual-band antennas, the following dual-band *decoupling conditions* must be satisfied within *two* frequency bands $[\omega_{L1}, \omega_{L2}]$ and $[\omega_{H1}, \omega_{H2}]$, whose center frequencies are ω_{L} and ω_{H}, respectively

$$\mathrm{Re}\left\{Y_{21}^A(\omega)\right\} \approx 0, \quad \omega \in [\omega_{L1},\ \omega_{L2}] \tag{2a}$$

$$j \cdot \mathrm{Im}\left\{Y_{21}^A(\omega)\right\} + Y_{21}^D(\omega) \approx 0, \quad \omega \in [\omega_{L1},\ \omega_{L2}] \tag{2b}$$

and

$$\mathrm{Re}\left\{Y_{21}^A(\omega)\right\} \approx 0, \quad \omega \in [\omega_{H1},\ \omega_{H2}] \tag{3a}$$

$$j \cdot \mathrm{Im}\left\{Y_{21}^A(\omega)\right\} + Y_{21}^D(\omega) \approx 0, \quad \omega \in [\omega_{H1},\ \omega_{H2}]\,. \tag{3b}$$

Assume that the two coupled antennas are both matched at the low and high bands. Using the S-to-Y transformation and conditions (2) and (3), the dual-band *matching conditions* can be written as

$$\mathrm{Re}\left\{Y_{kk}^A(\omega)\right\} \approx 1, \quad \omega \in [\omega_{L1},\ \omega_{L2}]\,, \quad k = 1, 2 \tag{4a}$$

$$j \cdot \mathrm{Im}\left\{Y_{kk}^A(\omega)\right\} + Y_{kk}^D(\omega) \approx 0, \quad \omega \in [\omega_{L1},\ \omega_{L2}]\,, \quad k = 1, 2 \tag{4b}$$

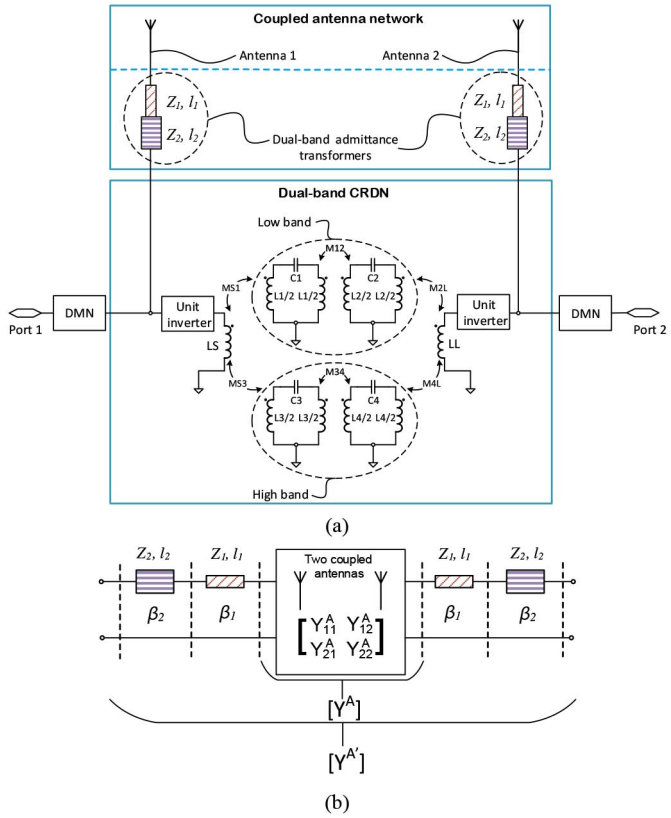

Fig. 1. (a) Circuit model of a two-port fourth-order dual-band CRDN in shunt with a two-port coupled antenna network together with a DMN. (b) Corresponding admittance matrices of the coupled antennas referenced before and after the admittance transformer.

and

$$\mathrm{Re}\left\{Y_{kk}^A(\omega)\right\} \approx 1, \quad \omega \in [\omega_{H1},\ \omega_{H2}]\,, \quad k = 1, 2, \text{ and} \tag{5a}$$

$$j \cdot \mathrm{Im}\left\{Y_{kk}^A(\omega)\right\} + Y_{kk}^D(\omega) \approx 0, \quad \omega \in [\omega_{H1},\ \omega_{H2}]\,, \quad k = 1, 2. \tag{5b}$$

It is worth mentioning that a unique feature of a CRDN is that the matching and the decoupling conditions can be well satisfied simultaneously. Nevertheless, to further enhance the matching performance, extra matching networks always help.

B. Admittance Transformer for Dual-Band Phase Shifting

To best satisfy conditions (2a) and (3a) simultaneously, the complex mutual admittances of the coupled antenna $Y_{21}^A(\omega)$ must be transformed to a purely imaginary number at the center frequency of the bands of interest while maintaining good impedance matching at the two ports. For a single-band application, it is already shown in [7] that with a section of uniform transmission line added to each port, the mutual admittance $Y_{21}^A(\omega)$ of a pair of coupled antennas can be transformed to a purely imaginary number at a specific frequency. To decouple two dual-band antennas, the phase shifting must be incorporated at two frequencies to achieve imaginary mutual admittance at two center frequencies in the band of interest.

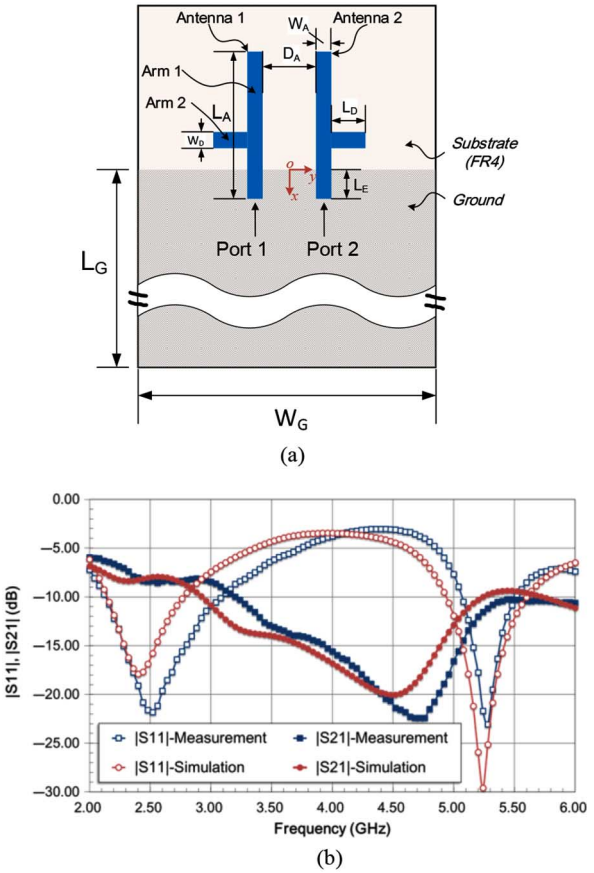

Fig. 2. (a) Layout of two coupled dual-band antennas. (b) Simulated and measured S-parameters of the coupled antennas.

In this work, a two-section stepped-impedance transformer will be used to accomplish this task.

In general, a two-section stepped-impedance transformer is formed by two transmission line sections with characteristic impedances Z_1 and Z_2 and physical lengths of l_1 and l_2, respectively. To simplify the design, $Z_1 = Z_0$ is chosen, where Z_0 is the references port impedance. Define $r = (Z_2 - Z_0)/(Z_2 + Z_0)$ as the ratio of the two characteristic impedances. It is found that by slightly varying r value, one can adjust the phase shift at the two bands independently in certain extent without scarifying the matching condition too much. Therefore, the r value together with l_1 and l_2 can be optimized to satisfy the required phase conditions in the two bands with minimum matching degradation.

As illustrated in Fig. 1(b), the admittance parameters of the original coupled antennas $\mathrm{Y^A}$ is transformed to admittances $\mathrm{Y}^{A'}$ by the two-section stepped-impedance transformer. Setting the real part of $\mathrm{Y}_{21}^{A'}$ to zero at frequencies ω_{L0} and ω_{H0}, which are the center frequencies of the two bands, yields two transcendental equations, which are not convenient to solve analytically. Nevertheless, the solution can be obtained using a simple optimization tool in advanced design system [21]. To illustrate the process, a pair of practical dual-band monopole antennas as shown in Fig. 2(a) is used as an example. The two identical printed dual-band monopoles are placed close to each other on a 1.6-mm-thick FR4 substrate. The separation distance $\mathrm{D_A} = 9.8\,\mathrm{mm}$, which is less than 0.077 λ_0 at 2.45 GHz and

TABLE I
DIMENSIONS OF COUPLED AND DECOUPLED ANTENNAS (mm)

Variable	Value	Variable	Value
$\mathrm{L_G}$	80.0	G, $\mathrm{G_R}$	0.3
$\mathrm{W_G}$	55.0	L	17.4
$\mathrm{L_A}$	30.0	W	3.8
$\mathrm{L_D}$	6.3	$\mathrm{W_T}$	2
$\mathrm{W_A}$	3.0	$\mathrm{F_R}$	0.4
$\mathrm{W_D}$	3.5	$\mathrm{W_B}$	4.7
$\mathrm{L_E}$	5.0	$\mathrm{W_E}$	0.6
S	0.6	$\mathrm{W_C}$	1.9

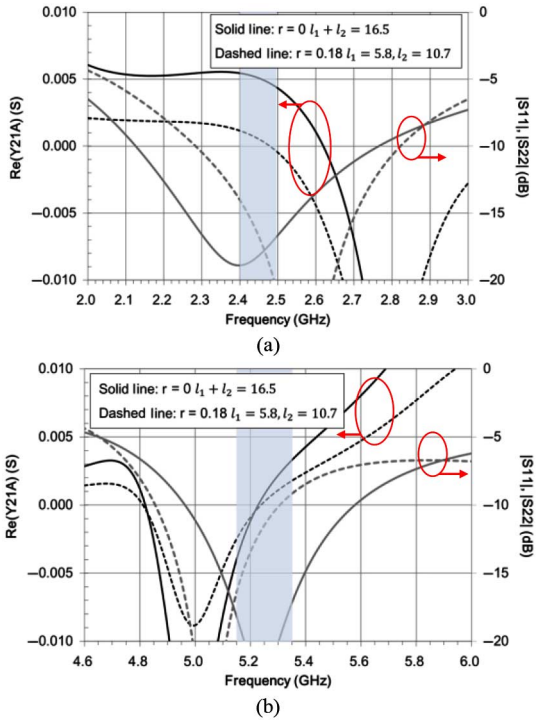

Fig. 3. Real part of mutual admittances (50-Ω termination) and return losses of coupled antennas for r = 0 and r = 0.18 at (a) the low band and (b) the high band.

0.17 λ_0 at 5.25 GHz. The simulated and measured scattering parameters of the coupled dual-band antennas are shown in Fig. 2(b). The isolation between the antennas is around $-8\,\mathrm{dB}$ at 2.45 GHz and $-10\,\mathrm{dB}$ at 5.25 GHz, while the two antennas are well matched in the two bands. Detailed dimensions of the test antennas are given in Table I.

To have a better understanding on the performance of the admittance transformer, parameters *r,* l_1, and l_2 are designed to best satisfy conditions (2a) and (3a) while maintaining a good matching condition within the two bands. The resultant real part of mutual admittance and the respective return losses are obtained by ADS and are shown in Fig. 3. As compared to the uniform transmission line case ($r = 0$) that only can fulfill (3a), a better solution for the two bands in this study is $r = 0.18$, $l_1 = 5.8\,\mathrm{mm}$, and $l_2 = 10.7\,\mathrm{mm}$ with the respective propagation constant specified by the FR4 substrate. As presented in Fig. 3, the real part of the transformed mutual admittance and the matching conditions after transformation using the solution meet the requirements satisfactorily. It will be shown later that the degradation in matching caused by

the transformer can always be compensated by a dual-band matching network (DMN).

C. Proposed Dual-Band CRDN

Since a CRDN shares many common features with coupled resonator type of filters, many matured dual-band filter design techniques can be utilized [22]. However, unlike specifying a dual-band filter in terms of S-parameters, the requirements for a CRDN are imposed on admittance parameters.

The circuit model of the proposed dual-band CRDN is shown in Fig. 1(a), which is quite similar to the circuit model of a single-band CRDN [11]. In both the low- and high-frequency bands, the relation between the coupling coefficients and the admittance parameter of the dual-band CRDN can be found from the nodal circuit analysis. According to [11], the inter-resonator coupling m_{12} has to be designed as large as the physical implementation allows. This conclusion is also valid for the dual-band scenario. Having fulfilled this requirement, the mutual admittances of the CRDN can remain nearly *constant* in a relatively large frequency band and can be written as [11]

$$y_{21}^{D}(\omega) \approx -j\frac{m_{S1}\cdot m_{2L}}{Z_0\cdot m_{12}}, \quad \omega\in[\omega_{L1},\ \omega_{L2}] \tag{6}$$

where m_{S1} and m_{2L} are the coupling coefficients of source to resonator 1 and resonator 2 to load, respectively. The self-admittances can be simplified to

$$y_{11}^{D}(\omega) = y_{22}^{D}(\omega) \approx 0, \quad \omega\in[\omega_{L1},\ \omega_{L2}] \tag{7}$$

which means that the CRDN is naturally matched near the center frequency.

By the same token, the admittance parameters at the high band can also be found to be

$$y_{21}^{D}(\omega) \approx -j\frac{m_{S3}\cdot m_{4L}}{Z_0\cdot m_{34}}, \quad \omega\in[\omega_{H1},\ \omega_{H2}] \tag{8}$$

and

$$y_{11}^{D}(\omega) = y_{22}^{D}(\omega) \approx 0, \quad \omega\in[\omega_{H1},\ \omega_{H2}] \tag{9}$$

where m_{34}, m_{S3}, and m_{4L} are the coupling coefficients of resonator 3 to resonator 4, source to resonator 3, and resonator 4 to load, respectively. It is obvious from (6) and (8) that the absolute value of y_{21}^{D} is mainly determined by the input and output couplings when the coupling between two coupled resonators is preset. The sign of y_{21}^{D} is controlled by the sign of inter-resonator coupling m_{12} and m_{34}. All these parameters need to be designed properly for a given coupled antenna pair according to (2b) and (3b). Moreover, it is obvious from (7) and (9) that the matching conditions (4b) and (5b) are naturally satisfied for a dual-band CRDN with matched antennas.

To understand the functions of all the coupling coefficients, four combinations of coupling coefficients of the dual-band CRDN shown in Table II are analyzed:

Case 1: a CRDN with opposite inter-resonator coupling coefficients at low and high band ($m_{12} = -m_{34}$);

Case 2: a CRDN with the same inter-resonator coupling coefficients at low and high band ($m_{12} = m_{34}$);

TABLE II
COUPLING COEFFICIENTS OF CASES 1–4 IN FIG. 5

	m_{S1}, m_{2L}	m_{12}	m_{S3}, m_{4L}	m_{34}
Case 1	1.0368	–2.5000	1.0368	2.5000
Case 2	1.0368	–2.5000	1.0368	–2.5000
Case 3	1.4663	–2.5000	1.4663	–2.5000
Case 4	0.7332	–1.2500	0.7332	–1.2500

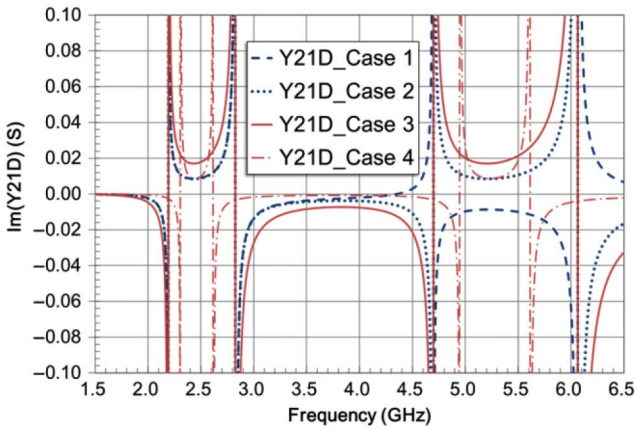

Fig. 4. Mutual admittances of a dual-band CRDN with different coupling coefficients in the case studies.

Case 3: a CRDN with larger input/output coupling coefficients at low and high band;

Case 4: a CRDN with small inter-resonator coupling coefficients at low and high band.

As shown in Fig. 4, the comparison between Case 1 and Case 2 is consistent with (6) and (8) in that the sign of y_{21}^{D} is determined by the sign of m_{12} and m_{34}; the comparison between Cases 2 and 3 illustrates that the absolute value of y_{21}^{D} is mainly controlled by the input/output couplings; the comparison between Cases 3 and 4 reveals the fact that the inter-resonator couplings have to be designed as large as possible for a relative flat y_{21}^{D} within the bands of interest.

III. DESIGN EXAMPLE

To validate the design theory and to prove the concept, a microstrip version of the proposed dual-band CRDN is designed and tested to decouple the two dual-band coupled monopole antennas depicted in Fig. 2(a).

The simulated S-parameters of the coupled antennas in this design example are shown in Fig. 2(b). A two-section stepped-impedance transformer is designed in the first step using the method discussed in Section II-B. The designed parameters of the transformer are listed in Table III. By introducing the stepped-impedance transformer, the real part of the mutual admittance $\mathrm{Re}\left(\mathrm{Y}_{21}^{A'}\right)$ becomes zero at both 2.45 and 5.25 GHz as shown in Fig. 5.

The two coupled antennas with the stepped-impedance transformer are connected to the dual-band CRDN in shunt to cancel out the imaginary part of the mutual admittance in both low and high bands. It can be seen from Fig. 5 that $\mathrm{Im}\left(Y_{21}^{A'}\right) = -0.0086$ at 2.45 GHz and $\mathrm{Im}\left(Y_{21}^{A'}\right) = 0.0066$

TABLE III
PARAMETERS OF THE DESIGNED STEPPED-IMPEDANCE TRANSFORMERS

	Electrical parameters		Physical dimensions (mm)	
	Z_0 (Ω)	θ (degree)	Width (w)	Length (l)
Section 1	50	31	3	5.8
Section 2	72	55	1.55	10.7
Section 3	50	34.5	3	6.5
Section 4	67	20.4	1.83	4
Section 5	48	32	3.3	6

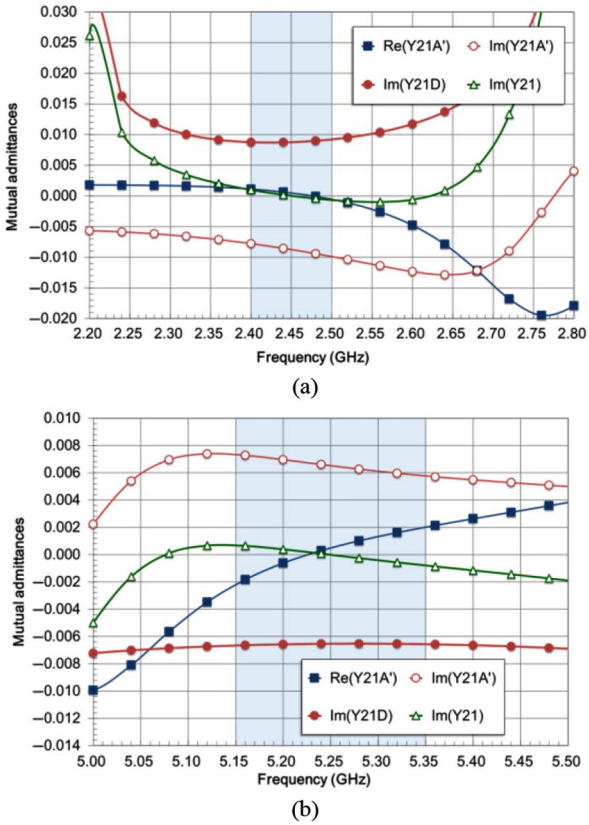

Fig. 5. Simulated mutual admittance parameters of the coupled antennas with and without the admittance transformer, and simulated mutual admittance parameters of the CRDN at (a) the low band and (b) the high band.

TABLE IV
COUPLING COEFFICIENTS OF DESIGNED AND REALIZED CRDN
(FBW = 10%)

	m_{S1}, m_{2L}/ m_{S3}, m_{4L}	m_{12}/m_{34}	m_{11}, m_{22}/ m_{33}, m_{44}
Designed (low band)	1.0368	–2.5000	0.0000
Realized (low band)	1.1267	–2.6798	–0.0051
Designed (high band)	0.9083	2.5000	0.0000
Realized (high band)	1.0288	2.7312	0.1123

at 5.25 GHz. It is interesting to note that the imaginary part of the mutual admittance between two dual-band coupled antennas is in opposite sign in the two frequency bands in this example. Meanwhile, in the low band (2.4–2.48 GHz) as well as the high band (5.15–5.35 GHz), the variation of $\mathrm{Im}\left(Y_{21}^{A'}\right)$

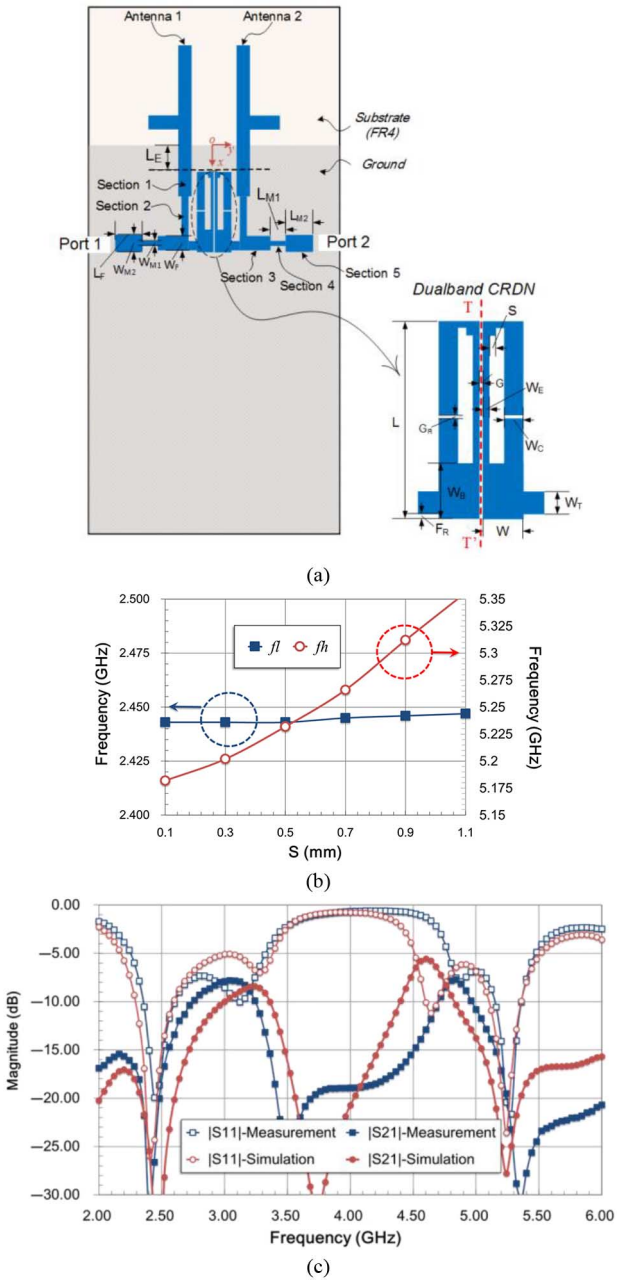

Fig. 6. (a) Layout of the dual-band CRDN and the dual-band antennas with the CRDN. (b) Resonant frequency of fundamental mode fl and resonant frequency of the second mode fh of the dual-band resonator against the size of the square perturbation element. (c) Simulated and measured S-parameters of the decoupled antennas.

is not more than $\pm 10\%$ Therefore, (2b) and (3b) can be further simplified as

$$Y_{21}^{D}(\omega) = -j\mathrm{Im}\left\{Y_{21}^{A}(\omega)\right\} \approx -j\mathrm{Im}\left\{Y_{21}^{A}(\omega_L)\right\}, \quad \omega \in [\omega_{L1},\ \omega_{L2}] \tag{10a}$$

and

$$Y_{21}^{D}(\omega) = -j\mathrm{Im}\left\{Y_{21}^{A}(\omega)\right\} \approx -j\mathrm{Im}\left\{Y_{21}^{A}(\omega_H)\right\}, \quad \omega \in [\omega_{H1},\ \omega_{H2}]. \tag{10b}$$

Based on (10), the coupling coefficients are obtained from (6) and (8) for both the low and high bands and are listed in

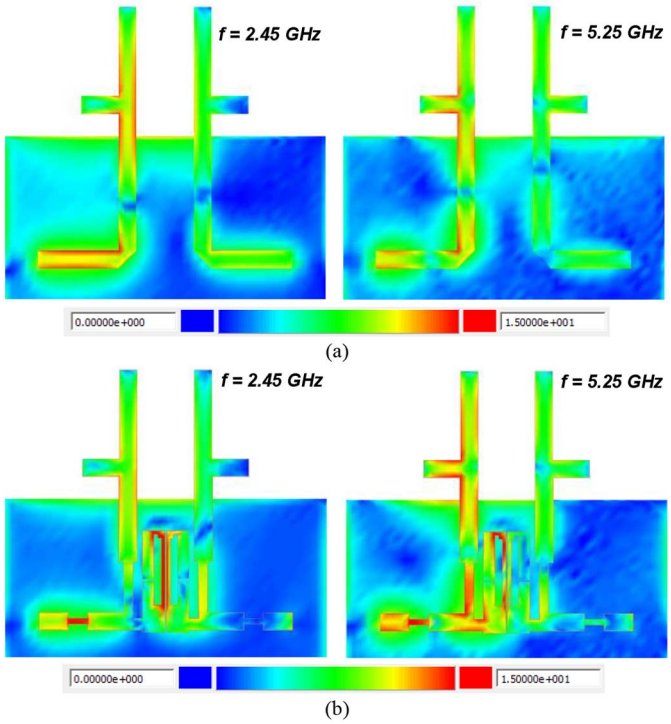

Fig. 7. Simulated current distribution of: (a) two coupled dual-band antennas at 2.45 and 5.25 GHz; and (b) same antennas decoupled by the dual-band CRDN at 2.45 and 5.25 GHz. In both cases, the element on left is excited and the element on right is terminated by a matched load.

Table IV. In fact, there are plenty of ways to realize a dual-band resonator using a multilayer PCB board. The dual-band open-loop square ring microstrip resonator in [22], as shown in Fig. 6(a), is used in light of its attractive features such as easy to be implemented by a planar circuit and compact in size. With the dual-band loop, the fundamental mode is used for the low-frequency band and the second harmonic mode is used for the high-frequency band.

The resonant frequency of the second harmonic mode can be perturbed by a small square corner with the size of S by S (mm^2) while nearly maintaining the resonant frequency of the fundamental mode unchanged as is shown in Fig. 6(b). The input couplings are implemented by the tapped-line scheme. A larger dimension of F_R will result in a smaller input/output coupling. The inter-resonator coupling is controlled by edge-to-edge distance, which is mainly magnetic coupling at the fundamental frequency. To keep this coupling as large as possible, the line width W_E and the gap size G have to be as small as the realization permits. The realized coupling coefficients are also listed in Table IV and the realized dimensions of the dual-band CRDN are already shown in Table I. As required by the mutual admittance of the coupled dual-band antennas, the coupling of the fundamental modes of the dual-band resonators is positive and the coupling between the second harmonic modes is negative. This can be justified by calculating the resonant frequencies of f_E and f_M when the symmetrical wall T–T' shown in Fig. 6(a) is replaced with an electric wall and magnetic wall, respectively. It is found that $f_E > f_M$ for the low band and $f_E < f_M$ for the high band.

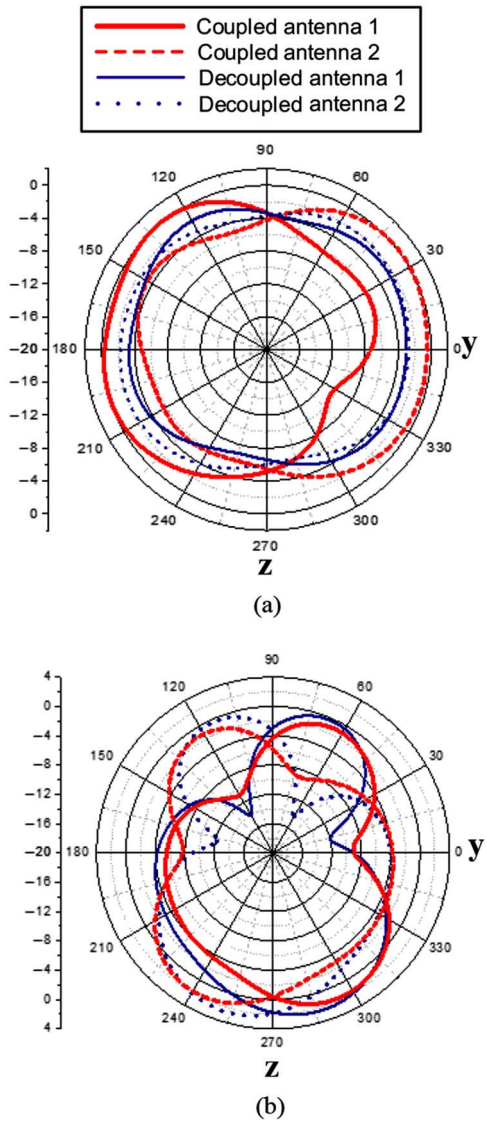

Fig. 8. Radiation patterns for the coupled and decoupled antennas in the yoz plane at (a) 2.45; and (b) 5.25 GHz.

It can be seen from S-parameters shown in Fig. 6(c) that, in the bands of interest, the designed CRDN significantly reduces the mutual couplings of the original coupled antennas in the two designated frequency bands as compared to those of the original coupled antennas shown in Fig. 2(b). To further improve the matching performance, another stepped-impedance transformer is designed with detailed dimensions listed in Table III as a DMN. The measured S-parameters shown in Fig. 6(c) demonstrate that the isolation between the decoupled antennas are more than 15 dB, while the return losses for both antennas are better than 10 dB in both 2.4–2.5-GHz band and 5.15–5.35-GHz band.

To reveal the decoupling mechanism, the simulated current distributions for the coupled and decoupled antenna arrays at both low and high bands using the method of moments solver in Agilent's advanced design system [21] are presented in Fig. 7. It is seen that a strong coupling between antennas is cancelled out by the current induced through the dual-band CRDN in the two frequency bands.

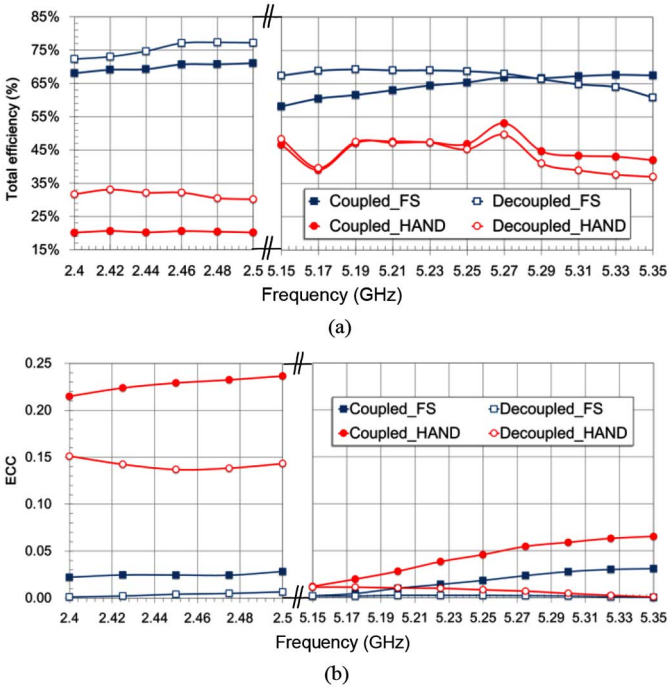

Fig. 9. (a) Measured total efficiencies, and (b) measured ECCs (absolute value) of coupled and decoupled dual-band antennas in FS and with hand phantom (HAND).

The radiation performances of the decoupled antennas in Fig. 6(a) and its coupled counterpart in Fig. 2(a) are also measured using the in-house SATIMO SG128 spherical near-field scanner [23] in an ISO17025 accredited laboratory. The radiation power patterns of both coupled and decoupled antennas are given in Fig. 8 for both low and high bands. Their total efficiencies are compared in Fig. 9(a). In the low band, the decoupled antenna pair has an improvement of around 3%–9% on top of about 70% in total efficiency, while in the high band, the improvement in total efficiency is not very obvious since the dielectric losses in the FR4 substrate tend to be dominant in the high band (5.2 GHz). It is expected that using a low-loss substrate can improve the efficiency more obviously, especially in the high band.

The envelope correlation coefficient (ECC) of the two antennas obtained from the measured complex far-field patterns over a sphere is an important figure of merit for benchmarking the performance of two coupled antennas in a Rayleigh fading channel. The coefficient is defined as [24]

$$\rho_e = \frac{\left| \iint\limits_{4\pi} [\vec{E_1}(\theta,\phi) \cdot \vec{E_2}(\theta,\phi)] d\Omega \right|^2}{\iint\limits_{4\pi} |\vec{E_1}(\theta,\phi)|^2 d\Omega \iint\limits_{4\pi} |\vec{E_2}(\theta,\phi)|^2 d\Omega} \tag{11}$$

where

$$\vec{E_1}(\theta,\phi) \cdot \vec{E_2}(\theta,\phi) = E_{\theta 1}(\theta,\phi) E^*{}_{\theta 2}(\theta,\phi) + E_{\phi 1}(\theta,\phi) E^*{}_{\phi 2}(\theta,\phi). \tag{12}$$

$\vec{E_i}(\theta,\phi)$ is the electric field radiated by antenna i with another antenna terminated by a matched load.

It is known that a lower envelope correlation leads to a larger channel capacity. As demonstrated by Fig. 9(b), in the case of free space (FS), the decoupled antenna pair has its ECC improved from 0.02 to 0.004 in the low band and 0.02 to 0.002 in the high band as compared to its coupled counterpart.

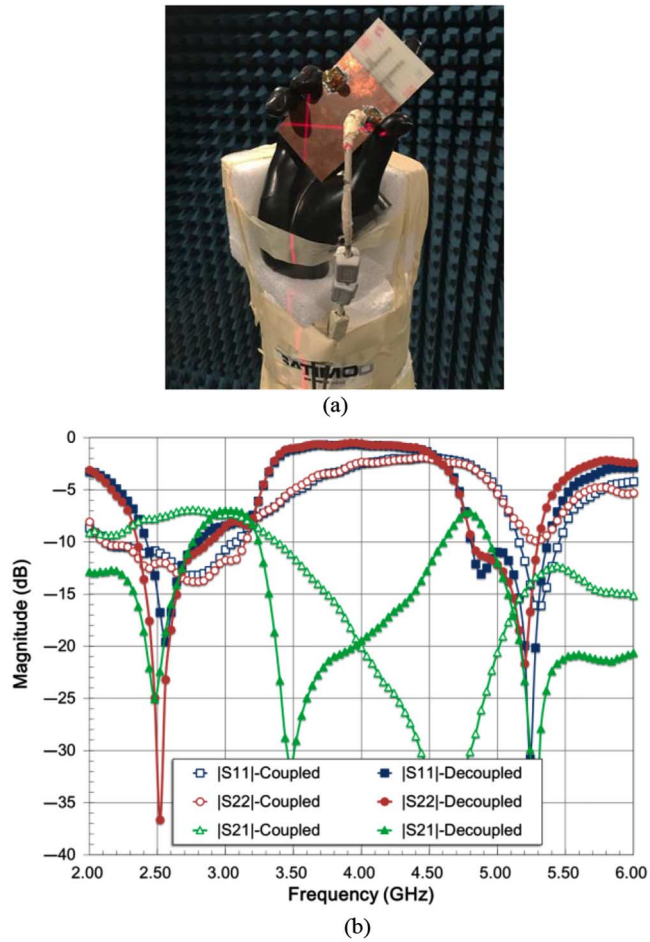

Fig. 10. (a) Measurement setup for antennas with hand phantom. (b) Measured scattering parameters of coupled and decoupled arrays with hand phantom.

In real-world applications, MIMO antennas suffer from the interferences from human body, especially the hands. To have a better insight on the performance of the decoupled antennas with hand interactions, the SPEAG hand phantom for monoblock phones SHO V2RB/LB is used [25] to emulate the hand effect with experiment setup shown in Fig. 10(a). The S-parameters for the coupled and decoupled antenna arrays shown in Figs. 2(a) and 6(a) are superposed in Fig. 10(b).

Since the hand phantom acts as a lossy dielectric medium in close proximity of the antennas, the resonant frequencies for all antennas, regardless of coupled and decoupled, are shifted and deteriorated.

The measured total efficiencies and ECCs for the coupled and decoupled array with hand phantom are also shown in Fig. 9. It is understandable that the total efficiencies drop significantly for both coupled and decoupled arrays due to the lossy nature of the hand. Nevertheless, the decoupled array still shows around 10% improvement in efficiency in the low band. The decoupled antenna pair has its ECC improved from 0.23 to 0.13 in the low band and 0.04 to 0.008 in the high band as compared to its coupled counterpart.

IV. Conclusion

A *dual-band* CRDN is proposed in this paper. The network aims at mitigating the strong mutual coupling between two dual-band antennas. A complete design theory of a dual-band CRDN and a practical realization in a planar microstrip form are presented in this paper. The network is compact in size and cost-effective in implementation. Although a pair of symmetric array is used in discussion, the decoupling approach is general for any antenna form factors including asymmetric arrays. While reducing the unwanted mutual couplings, the CRDN also provides a good matching performance, which makes it very promising to be used in an MIMO system in a wireless terminal. The research on an integrated module of the proposed CRDN network for decoupling of two dual-band antennas is on the way.

References

[1] Z. N. Chen, X. N. Low, and T. S. P. See, "Analysis and optimization of compact suspended plate MIMO antennas," *IEEE Trans. Antennas Propag.*, vol. 59, no. 1, pp. 263–270, Jan. 2011.

[2] J. C. Coetzee and Y. Yu, "Port decoupling for small arrays by means of an eigenmode feed network," *IEEE Trans. Antennas Propag.*, vol. 56, no. 6, pp. 1587–1593, Jun. 2008.

[3] C. Volmer, J. Weber, R. Stephan, K. Blau, and M. A. Hein, "An eigen-analysis of compact antenna arrays and its application to port decoupling," *IEEE Trans. Antennas Propag.*, vol. 56, no. 2, pp. 360–370, Feb. 2008.

[4] J. Weber, C. Volmer, K. Blau, R. Stephan, and M. A. Hein, "Miniaturized antenna arrays using decoupling networks with realistic elements," *IEEE Trans. Microw. Theory Technol.*, vol. 54, no. 6, pp. 2733–2740, Jun. 2006.

[5] L. K. Yeung and Y. E. Wang, "Mode-based beamforming arrays for miniaturized platforms," *IEEE Trans. Microw. Theory Technol.*, vol. 57, no. 1, pp. 45–52, Jan. 2009.

[6] J. B. Andersen and H. H. Rasmussen, "Decoupling and descattering networks for antennas," *IEEE Trans. Antennas Propag.*, vol. 24, no. 6, pp. 841–846, Nov. 1976.

[7] S. Chang, Y.-S. Wang, and S.-J. Chung, "A decoupling technique for increasing the port isolation between strongly coupled antennas," *IEEE Trans. Antennas Propag.*, vol. 56, no. 12, pp. 3650–3658, Dec. 2008.

[8] A. Diallo, C. Luxey, P. L. Thuc, R. Staraj, and G. Kossiavas, "Study and reduction of the mutual coupling between two mobile phone PIFAs operating in the DCS1800 and UMTS bands," *IEEE Trans. Antennas Propag.*, vol. 54, no. 11, pp. 3063–3073, Nov. 2006.

[9] F. Yang and Y. R. Samii, "Microstrip antennas integrated with electromagnetic band-gap EBG structures: A low mutual coupling design for array applications," *IEEE Trans. Antennas Propag.*, vol. 51, no. 10, pp. 2936–2946, Oct. 2003.

[10] C. Y. Chiu, C. H. Cheng, R. D. Murch, and C. R. Rowell, "Reduction of mutual coupling between closely-packed antenna element," *IEEE Trans. Antennas Propag.*, vol. 55, no. 6, pp. 1732–1738, Jun. 2007.

[11] L. Zhao, L. K. Yeung, and K.-L. Wu, "A coupled resonator decoupling network for two-element compact antenna arrays in mobile terminals," *IEEE Trans. Antennas Propag.*, vol. 62, no. 5, pp. 2767–2776, May 2014.

[12] L. Zhao and K.-L. Wu, "A broadband coupled resonator decoupling network for a three-element compact array," in *Proc. IEEE MTT-S Int. Microw. Symp.*, Jun. 2013, pp. 1–3.

[13] M. S. Sharawi, A. B. Numan, M. U. Khan, and D. N. Aloi, "A dual-element dual-band MIMO antenna system with enhanced isolation for mobile terminals," *IEEE Antennas Wireless Propag. Lett.*, vol. 11, pp. 1006–1009, Aug. 2012.

[14] Y. Ding, Z. Du, K. Gong, and Z. Feng, "A novel dual-band printed diversity antenna for mobile terminals," *IEEE Trans. Antennas Propag.*, vol. 55, no. 7, pp. 2088–2096, Jul. 2007.

[15] X. M. Ling and R. L. Li, "A novel dual-band MIMO antenna array with low mutual coupling for portable wireless devices," *IEEE Antennas Wireless Propag. Lett.*, vol. 10, no. 1, pp. 1039–1042, Sep. 2011.

[16] X. Tang, K. Mouthaan, and J. C. Coetzee, "Dual-band decoupling and matching network design for very closely spaced antennas," in *Proc. Eur. Microw. Conf.*, 2012, pp. 49–52.

[17] C.-Y. Lui, Y.-S. Wang, and S.-J. Chung, "Two nearby dual-band antennas with high port isolation," presented at the IEEE Antennas Propag. Symp. Dig., San Diego, CA, USA, Jul. 2008.

[18] P.-L. Chi, C.-J. Lee, and T. Itoh, "A compact dual-band metamaterials-based rat-race coupler for a MIMO system application," in *Proc. IEEE MTT-S Int. Microw. Symp. Dig.*, Jun. 15–20, 2008, pp. 667–670.

[19] P. Chi and T. Itoh, "Miniaturized dual-band directional couplers using composite right/left-handed transmission structures and their applications in beam pattern diversity systems," *IEEE Trans. Microw. Theory Technol.*, vol. 57, no. 5, pp. 1207–1215, May 2009.

[20] K.-C. Lin, C.-H. Wu, C.-H. Lai, and T.-G. Ma, "Novel dual-band decoupling network for two-element closely spaced array using synthesized microstrip lines," *IEEE Trans. Antennas Propag.*, vol. 60, no. 11, pp. 5118–5128, Nov. 2012.

[21] *Advanced Design System, Version 2012.08*, Agilent Technol. Inc., Santa Clara, CA, USA, 2012.

[22] J.-S. Hong and M. J. Lancaster, *Microstrip Filters for RF/Microwave Applications*, 2nd ed. Hoboken, NJ, USA: Wiley, 2011, ch. 7–10.

[23] [Online]. Available: http://www.satimo.com/

[24] R. G. Vaughan and J. B. Andersen, "Antenna diversity in mobile communications," *IEEE Trans. Veh. Technol.*, vol. 36, no. 4, pp. 149–172, Nov. 1987.

[25] [Online]. Available: http://www.speag.com/

Luyu Zhao (S'09–M'14) was born in Xi'an, China, in 1984. He received the B.Eng. degree from the Xidian University, Xi'an, China, in 2007, and the Ph.D. degree from The Chinese University of Hong Kong, Shatin, Hong Kong, in 2014, all in electrical engineering.

Currently, he is a Postdoctoral Fellow with The Chinese University of Hong Kong. From 2007 to 2009, he was a Research Assistant with the National Key Laboratory of Antennas and Microwave Technology, Xidian University, where he was involved with software and hardware implementation of RF identification (RFID) technologies. His research interests include design and application of multiple antenna systems for the next-generation mobile communication systems as well as innovative passive RF and microwave components, circuits, and systems.

Dr. Zhao was the recipient of the Best Student Paper Award of 2013 IEEE 14th HK AP/MTT Postgraduate Conference.

Ke-Li Wu (M'90–SM'96–F'11) received the B.S. and M.Eng. degrees from the Nanjing University of Science and Technology, Nanjing, China, in 1982 and 1985, respectively, and the Ph.D. degree from the Laval University, Quebec, QC, Canada, in 1989, all in electrical engineering.

From 1989 to 1993, he was a Research Engineer and a Group Manager with the Communications Research Laboratory, McMaster University, Hamilton, ON, Canada. In March 1993, he joined the Corporate R&D Division, COM DEV International, where he was a Principal Member of Technical Staff. Since October 1999, he has been with The Chinese University of Hong Kong, Shatin, Hong Kong, where he is a Professor and the Director of the Radiaofrequency Radiation Research Laboratory (R3L). His research interests include partial element equivalent circuit (PEEC) and derived physically expressive circuit (DPEC) EM modeling of high-speed circuits, RF and microwave passive circuits and systems, synthesis theory and practices of microwave filters, antennas for wireless terminals, LTCC-based multichip modules (MCMs), and RF identification (RFID) technologies.

Prof. Wu is a member of the IEEE MTT-8 subcommittee (Filters and Passive Components) and also serves as a TPC member for many prestigious international conferences including International Microwave Symposium. He was an Associate Editor of IEEE Transactions on MTT from 2006 to 2009. He was the recipient of the 1998 COM DEV Achievement Award for the development of exact EM design software of microwave filters and multiplexers and Asia Pacific Microwave Conference Prize in 2008 and 2012, respectively.